Dichroism of plasmonic chiral nanoalloys by rational design

Pierpaolo D'Antoni[1] | Daniele Toffoli[1] | Giovanna Fronzoni[1] | Mauro Stener[1] | Luca Sementa[2] | Alessandro Fortunelli[2]

[1]Dipartimento di Scienze Chimiche e Farmaceutiche, Università di Trieste, Trieste, Italy

[2]CNR-ICCOM & IPCF, Consiglio Nazionale delle Ricerche, Pisa, Italy

Correspondence
Mauro Stener, Dipartimento di Scienze Chimiche e Farmaceutiche, Università di Trieste, Via Giorgieri 1, 34127 Trieste, Italy.
Email: stener@units.it

Alessandro Fortunelli, CNR-ICCOM, Via Moruzzi 1, 56124 Pisa, Italy.
Email: alessandro.fortunelli@cnr.it

Funding information
Beneficentia Stiftung; ICSC—Centro Nazionale di Ricerca in High Performance Computing, Big Data and Quantum Computing; Università degli Studi di Trieste

Abstract

Time-dependent density functional theory (TDDFT) simulations are conducted on a series of chiral gold/silver alloy nanowires to explore whether silver doping can produce an enhancement of circular dichroism at the plasmon resonance in these systems, and to identify the quantum-mechanical origin of the observed effects. We find a strong plasmonic dichroism when one or two helixes of gold atoms are substituted by silver in a linear chiral nanotube, whose pure gold counterpart does not display any plasmonic dichroism, and we rationalize this finding in terms of "decoupling" the destructive interference of excitations in the pure gold nanotube via alloying. However, further attempts to increase the plasmonic dichroism by considering multi-shell gold nanowires in which one entire shell is doped with silver did not produce the desired effect, but rather a decrease in circular dichroism. We show that this latter result is due to a more severe destructive interference in the dipole excitation contributions, and suggest that further amplification should be possible in principle by properly tuning simultaneously the nanowire structure and chemical ordering.

KEYWORDS
chiral metal clusters, plasmonic dichroism

1 | INTRODUCTION

Plasmons play a major role in nanotechnology since they can focus the electromagnetic field within a small region of space thus obtaining a high electromagnetic energy density.[1–3] This effect can potentially amplify the local field intensity by many orders of magnitude and is routinely exploited in enhanced spectroscopies like Surface Enhanced Raman spectroscopy,[4] allowing the study of even single-molecules.[5,6] Although the nature of the plasmon phenomenon is well established for extended systems as an electronic collective oscillation mode, for finite nano-sized systems such as nanoclusters and nanowires their physical nature is still discussed and not yet completely assessed.[7–11]

Besides photoabsorption, when the system is chiral (absence of symmetry planes and inversion symmetry), an Electronic Circular Dichroism (ECD) signal is expected, that is, the absorption coefficient is different when right or left circularly polarized light is employed in the experiment. The ECD response can be exploited in practice for extremely selective chiral sensing.[12] However, the ECD signal is governed by the electric-dipole/magnetic-dipole scalar product, according to the Rosenfeld equation (Equation 1)[13]:

$$R_{on} = Im(\langle 0|\boldsymbol{\mu}|n\rangle\langle n|\boldsymbol{m}|0\rangle), \quad (1)$$

so ECD is much weaker than absorption, typically by a factor of about $\approx 10^{-5}$. Therefore the ability of amplifying the ECD exploiting *plasmonic* effects is a very promising strategy to improve the efficiency of chiral sensing and has been the topic of active research in the last decades.[14–17] Plasmonic ECD can be conveniently classified into structural and induced[17]: structural plasmonic ECD is related to systems which are intrinsically chiral,[18] while induced plasmonic ECD is generated by a chiral arrangement of non-chiral subsystems. Induced plasmonic ECD is more accessible at the experimental level,[19] but the growing interest for structural chiral plasmonics is justified by its potential larger enhancing efficiency and to the availability of new

synthetic strategies based on new bottom-up advanced techniques. From the theoretical point of view, it is important to identify which is the most suitable method to computationally describe the plasmon. When the system size is below 2 nm, such as gold clusters, quantum confinement effects are important,[20] and a quantum mechanical approach is necessary. Moreover, being the plasmon a collective resonance, it is necessary to employ a method which allows configuration mixing like Time Dependent Density Functional Theory (TDDFT),[21] while simpler DFT is not suitable.[22] In the present work we are interested in alloy nanosystems, whose relative small size still allows for a TDDFT treatment. In a previous work[23] some of us have shown that linear chiral gold nanowires exhibit very intense plasmonic absorption but almost negligible ECD despite being chiral. Additionally, it was shown that if the nanowires are coiled around the lateral surface of a cylinder the ECD is dramatically more intense than in linear nanowires. An analysis based on Individual Component Map of Rotatory Strength (ICM-RS)[24] demonstrated that in linear nanowires the plasmonic ECD is drastically quenched by an almost perfect *totally* destructive interference among iso-energetic configurations present in the collective plasmonic excitation. Hence, it was suggested that a small "perturbation" of the nanowire may be able to remove this almost perfect destructive interference and produce an intense plasmonic ECD. Coiling the nanowires indeed represents a kind of perturbation of the system shape. In the present paper we further elaborate this line of research, investigate a different route, and demonstrate that alloying may also be a practical way to avoid destructive interference and achieve a *plasmonic ECD signal* even in strictly linear nanowires.

The article is organized as follows. In Section 2, we give a brief description of the computational method. In Section 3, we report the results and their discussion for two kinds of linear nanoalloys which differ by their chemical ordering. In the first class of linear nanoalloys one or more chains of coiling atoms are doped, whereas in the second class of linear nanowires one entire wall (or shell) is doped within a multiwall systems. Interestingly, we obtain a strong plasmonic ECD only for the former class of doped systems, and we rationalize our finding via an analysis of ICM plots and induced densities. Finally, Section 4 summarizes the conclusions of the present study.

2 | THEORETICAL METHOD AND COMPUTATIONAL DETAILS

The geometries of the systems considered in the present study were taken from our previous work on gold nanowires,[23] by only changing the nature of the element, that is, replacing gold atoms with silver ones while keeping the original coordinates, not allowing for geometrical relaxation. This choice is justified since gold and silver have an almost identical atomic radius, of 1.46 and 1.44 Å, respectively, and we are interested in fundamental phenomena in pure form, without complications due to structural effects.

Photoabsorption as well as ECD calculations were carried out with the complex polarizability TDDFT (pol-TDDFT) algorithm,[25,26] using the ADF engine of the AMS software.[27] Such method consists in a linear-response TDDFT formalism in the frequency domain.

The algorithm calculates the oscillator strength and the rotatory strength as:

$$f = \frac{2\omega\varepsilon}{3} Im[\bar{\alpha}] \; R = \frac{3\omega\varepsilon}{2c} Im[\bar{\beta}], \tag{2}$$

where, $Im[\bar{\alpha}]$ and $Im[\bar{\beta}]$ represent respectively the imaginary part of the polarizability and rotatory strength tensor averaged over all the orientations, ω is the photon energy, c is the speed of the light, and ε is the imaginary part of the photon energy chosen as 0.06 eV. We have chosen this value since it has been already employed in the previous works on gold nanowires,[22,23] this allows to compare consistently the present results with those ones. The calculations were done with the asymptotically corrected LB94 xc functional,[28] the TZP basis-set (with density fitting set appropriately optimized to be used with the pol-TDDFT[29]), and the scalar ZORA[30] approach. Such choice has proven as a convenient compromise between accuracy and computational economy: in particular both xc functional[31] and basis set performances[29] have been assessed in previous work.

Besides the calculation of photoabsorption and ECD, we also analyze the results using tools specifically developed to study plasmonic systems in previous work: the Individual Component Map of Oscillator Strength plots (ICM-OS)[32] and the Individual Component Map of Rotatory Strength plots (ICM-RS).[24]

2.1 | Nanoalloys structures and chemical ordering

The structures of the alloy nanowires considered in this work are reported in Figure 1.[23] Such structures were inspired by linear chiral nanowires produced experimentally.[33] In the present work, we used identical geometrical structures, but introducing a chemical substitution of a subset of gold atoms with silver ones. Note that we did not re-optimize the structures, this assumption being justified by the almost identical atomic radius of gold and silver, as well as their almost identical interatomic distance in the bulk. Starting from above and using the nomenclature adopted in the previous work,[23] Figure 1A ($Au_{122}Ag_{30}$) and Figure 1B ($Au_{90}Ag_{62}$) correspond to the (5,3)NT (NanoTube) where one or two gold wires were substituted by silver atoms respectively. The substitution were introduced in one or two of the five wires which, coiling around the longitudinal axis, constitute the (5,3)NT. In the case of Figure 1B ($Au_{90}Ag_{62}$) the two silver wires are chosen in order not to be adjacent, in fact there are only two possibilities to choose the two wires from five: adjacent or not adjacent. We took the non-adjacent chemical ordering in order to maximize the "perturbing" effects of alloying on destructive interference. In the other structures we explored the effect of alloying from a different perspective: instead of generating a coiling pattern on the exposed surface of the system, we alloyed different shells of a multi-shell system. For this reason we have taken the 7-1 Helical Multi Shell

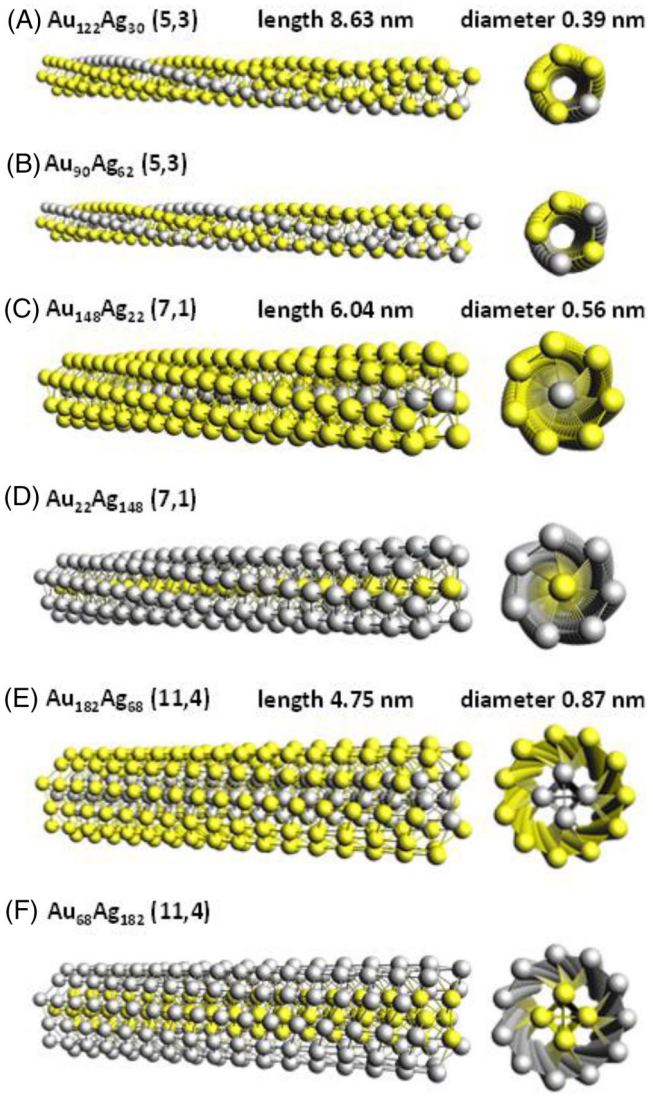

FIGURE 1 Structures of the nanoalloys considered in the present work. (5,3)NT: (A) $Au_{122}Ag_{30}$ and (B) $Au_{90}Ag_{62}$. 7-1 HMS (C) $Au_{148}Ag_{22}$ and (D) $Au_{22}Ag_{148}$. 11-4 HMS (E) $Au_{182}Ag_{68}$ and (F) $Au_{68}Ag_{182}$.

(HMS) and the 11-4 HMS. These systems consist of two shells: in 7-1 HMS seven nanowires are coiling around one linear chain of metal atoms which lies along the longitudinal axis of the system. In the 11-4 nanowire 11 wires are coiling around an achiral nanotube consisting of four linear wires. In present work, Figure 1C ($Au_{148}Ag_{22}$) and Figure 1D ($Au_{22}Ag_{148}$) correspond to the 7-1 HMS structure where the inner wire consists of silver and gold atoms respectively, and the atomic nature of the outer shell is opposite to the inner one. Figure 1E ($Au_{182}Ag_{68}$) and Figure 1F ($Au_{68}Ag_{182}$) instead correspond to the 11-4 HMS structure where the inner nanotube consists of silver and gold atoms, respectively, and the outer shell atomic nature is opposite to the inner one.

Note that in this study we do not investigate the dependence of plasmonic phenomena upon the size of the wires, which was the topic of a previous work.[22]

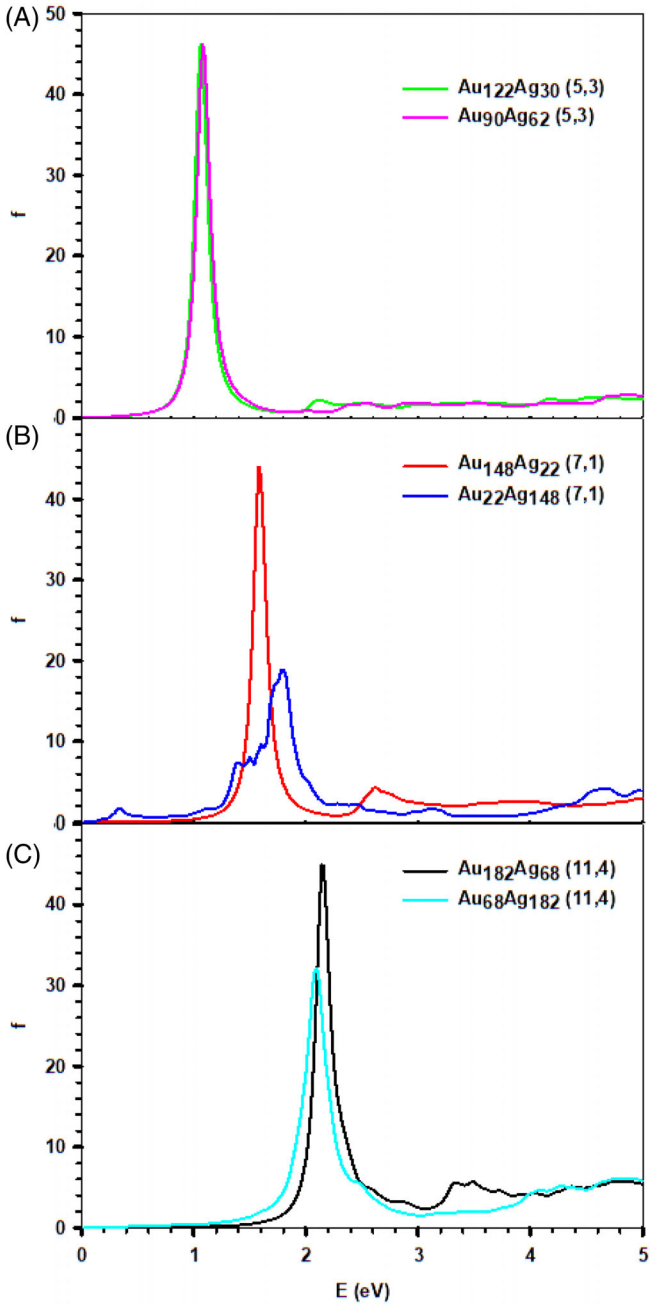

FIGURE 2 Photoabsorption for the series of linear chiral nanoalloys. (A) (5,3)NT $Au_{122}Ag_{30}$ and $Au_{90}Ag_{62}$. (B) 7-1 HMS $Au_{148}Ag_{22}$ and $Au_{22}Ag_{148}$. (C) 11-4 HMS $Au_{182}Ag_{68}$ and $Au_{68}Ag_{182}$.

3 | RESULTS AND DISCUSSION

3.1 | Nanoalloys plasmonic photoabsorption

In Figure 2, the calculated TDDFT photoabsorption spectra of all the systems defined in Section 2.1 are reported. All the calculated profiles display a very sharp and intense plasmonic peak whose energy is almost independent by the chemical ordering but changes with the structure. More precisely, the peak of (5,3)NT

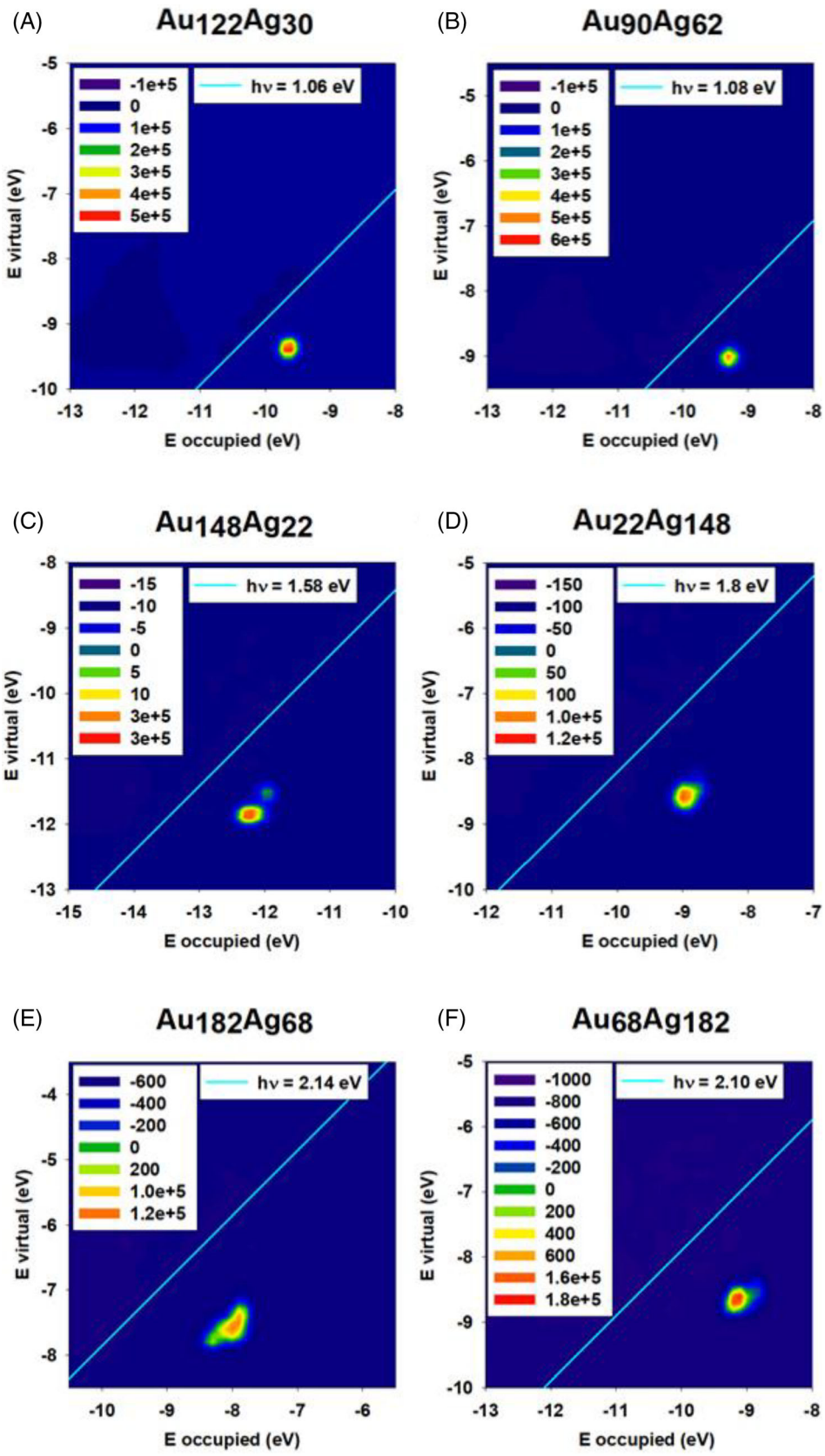

FIGURE 3 ICM-OS analysis of the longitudinal electric dipole component at plasmon energies for the nanoalloys: (A) $Au_{122}Ag_{30}$ at 1.06 eV, (B) $Au_{90}Ag_{62}$ at 1.08 eV, (C) $Au_{148}Ag_{22}$ at 1.58 eV, (D) $Au_{22}Ag_{148}$ at 1.80 eV, (E) $Au_{182}Ag_{68}$ at 2.10 eV, and (F) $Au_{68}Ag_{182}$ at 2.14 eV. The straight line corresponds to virtual-occupied pair energy difference equal to the excitation energy.

falls at 1.06 and 1.08 eV for $Au_{122}Ag_{30}$ and $Au_{90}Ag_{62}$, in 7-1 HMS the peak is at 1.58 and 1.80 eV for $Au_{148}Ag_{22}$ and $Au_{22}Ag_{148}$, finally in 11-4 HMS the plasmon lies at 2.14 and 2.10 eV for $Au_{182}Ag_{68}$ and $Au_{68}Ag_{182}$, respectively. The energies and the photoabsorption intensities of the plasmon resonances of the nanoalloys are quite close to those of the corresponding gold

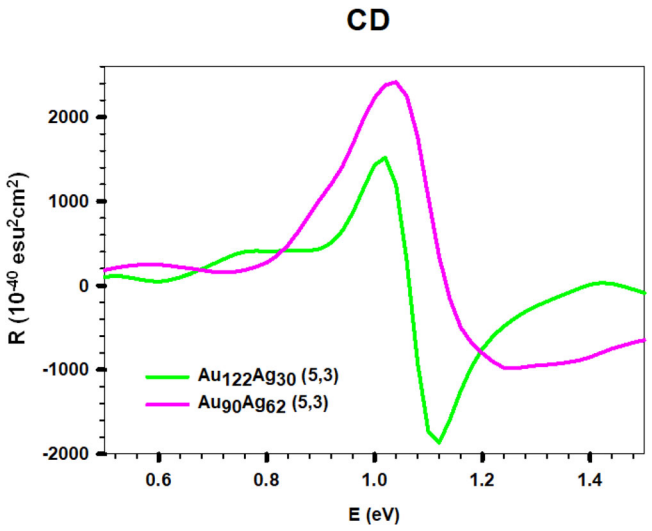

FIGURE 4 ECD for the linear chiral nanoalloys (5,3)NT $Au_{122}Ag_{30}$ and $Au_{90}Ag_{62}$. Rotator strength (R) is given in 10^{-40} esu^2 cm^2.

nanowires,[23] indicating that alloying has a negligible effect on the plasmonic resonance in absorption. Up to now we have ascribed the spectral features to plasmon resonances due to their sharp and intense peak. It is however desirable to confirm the plasmonic nature of such features via a more rigorous argument. To this end we employed the ICM-OS analysis, whose results are reported in Figure 3. In these plots, calculated at the energies corresponding to the maximum absorption and for the longitudinal dipole component, we report the energy of the occupied orbitals on the *x*-axis and the energy of the virtual ones on the *y*-axis. The "spots" correspond to the dipole contribution arising from the occupied-virtual pair excited configurations with orbital energies corresponding to the values of the *x* and *y* coordinates. The straight line corresponds to a virtual-occupied pair energy difference equal to the excitation energy. As it can be easily seen, all the spots are remarkably far (at least 1 eV) from the straight line, indicating a strong coupling between different configurations, confirming the plasmonic collective behavior of the peak.

FIGURE 5 On the left panel are shown the ICM-RS analysis of the longitudinal magnetic dipole component at plasmon energies for the (5,3)NT nanoalloys: (A) $Au_{122}Ag_{30}$ at 1.06 eV and (B) $Au_{90}Ag_{62}$ at 1.08 eV. In right panel the same plots are shown in 3D to better appreciate the destructive interference effect.

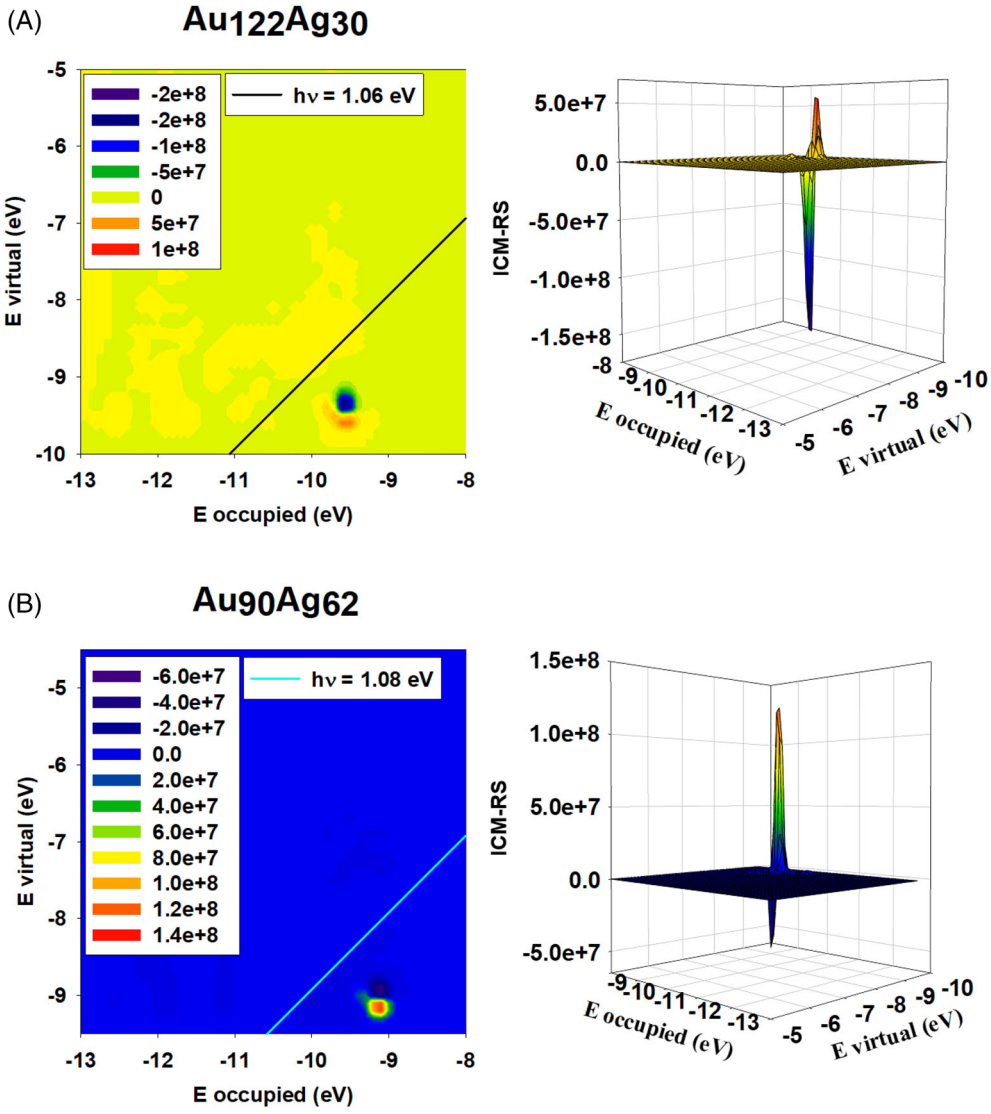

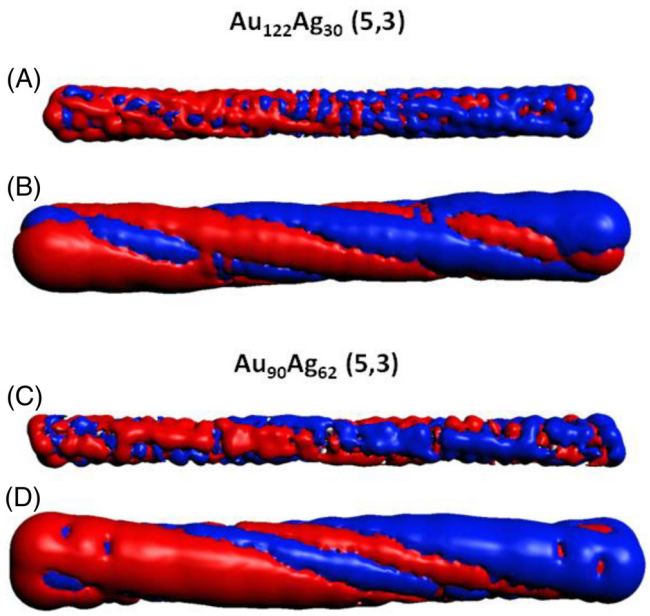

FIGURE 6 The induced density of the longitudinal component at plasmon energies for the (5,3)NT nanoalloys: (A, B) $Au_{122}Ag_{30}$ at 1.06 eV and (C, D) $Au_{90}Ag_{62}$ at 1.08 eV. The isosurface value is 0.03 electrons/Bohr^3 for (A and C) and 0.00003 electrons/Bohr^3 for (B and D).

3.2 | Nanoalloys plasmonic electronic circular dichroism of (5,3)NT

In Figure 4, we report the calculated TDDFT ECD of the two (5,3) NT nanoalloys. Surprisingly, it is immediately evident that a very intense ECD is calculated at the plasmon energy. It is worth noting that this finding is a genuine effect of alloying. Indeed, the pure gold (5,3)NT gave no ECD features at the plasmon resonance.[23] Morever the effect is quite strong, with a Rotator strength (R) amplified by a factor of about 20 as a consequence of alloying: from R around ±100 cgs 10^{-40} units of the background without plasmon enhancement of the pure gold nanowire[23] to R around ±2000 for the nanoalloys. Besides its intensity, it is apparent that such plasmonic ECD is also sensitive to the chemical ordering, as the spectral features are appreciably different in the two nanowires: the typical Cotton profile of $Au_{122}Ag_{30}$ is less positive than $Au_{90}Ag_{62}$ just below the plasmon energy, but is more negative above the plasmon. Moreover, also the curvature of the R profile is different just beyond the plasmon: $Au_{122}Ag_{30}$ displays a convex shape (corresponding to a negative second derivative) while $Au_{90}Ag_{62}$ gives a concave shape (positive second derivative), such behavior extending roughly from 1.0 to 1.5 eV. We believe that this finding is quite new and very promising in terms of potential applications and exploitations in the field of nanoscience. Indeed, the possibility to enhance ECD by alloying could be exploited to trigger ECD on presently inactive systems. Of course, taking complete control over the chemical ordering in such systems is challenging, but the potential chances it offers are so significant to trigger pursuing it. To the best of our knowledge, this is the first time

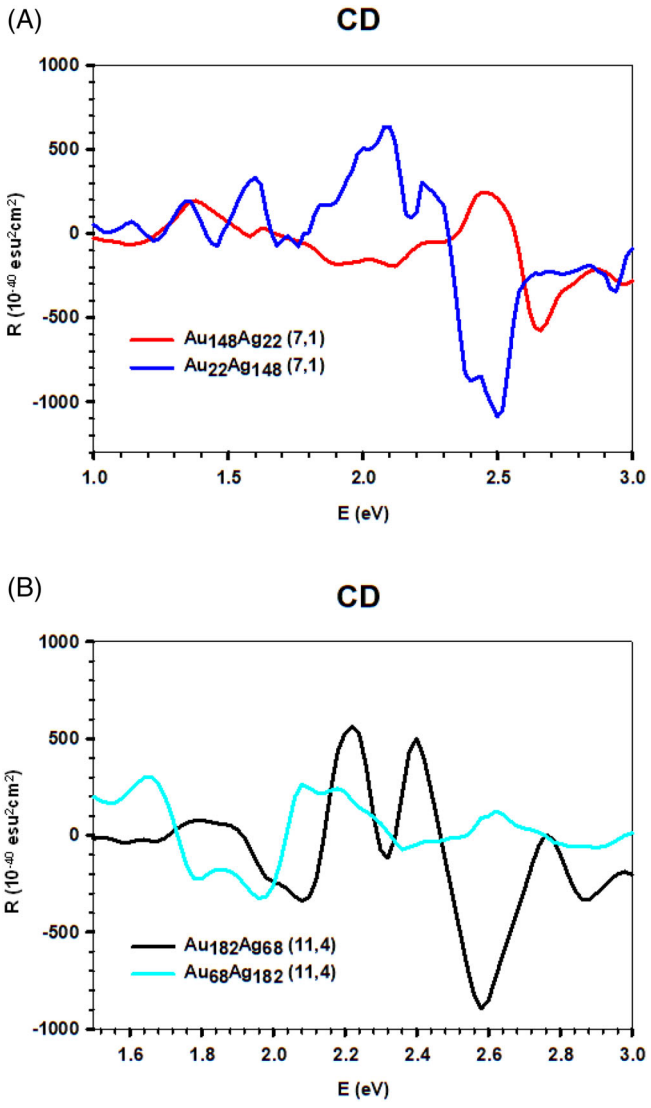

FIGURE 7 ECD for the linear chiral nanoalloys (A) 7-1 HMS $Au_{148}Ag_{22}$ and $Au_{22}Ag_{148}$, (B) $Au_{182}Ag_{68}$ and $Au_{68}Ag_{182}$. Rotator strength (R) is given in 10^{-40} esu^2 cm^2.

in which a chiral chemical ordered alloying is predicted to have such a dramatic effect on the ECD. It is clearly important from a scientific point of view to investigate the physical origin of this new effect, to understand better the mechanism lying behind it so as to suggest even more effective enhancements and finally reach a rational design of dichroic plasmonic nanoalloys. We have thus performed an ICM-RS analysis at the plasmon energies to better describe what happens in terms of electronic structure. The ICM-RS analysis is analogue to the ICM-OS one, but now the contributions of the excited configurations are weighted by the magnetic dipole transition moment, in order to split the total R in contributions from each one-electron excited pair. In the ICM-RS the electric dipole is used as an external field perturbation, the induced magnetic dipole is calculated by linear response. The ICM-RS analysis at the plasmon energies of $Au_{122}Ag_{30}$ and $Au_{90}Ag_{62}$ are reported in Figure 5. It is well apparent that both systems display a strong dichroism which is the sum of two contributions of opposite

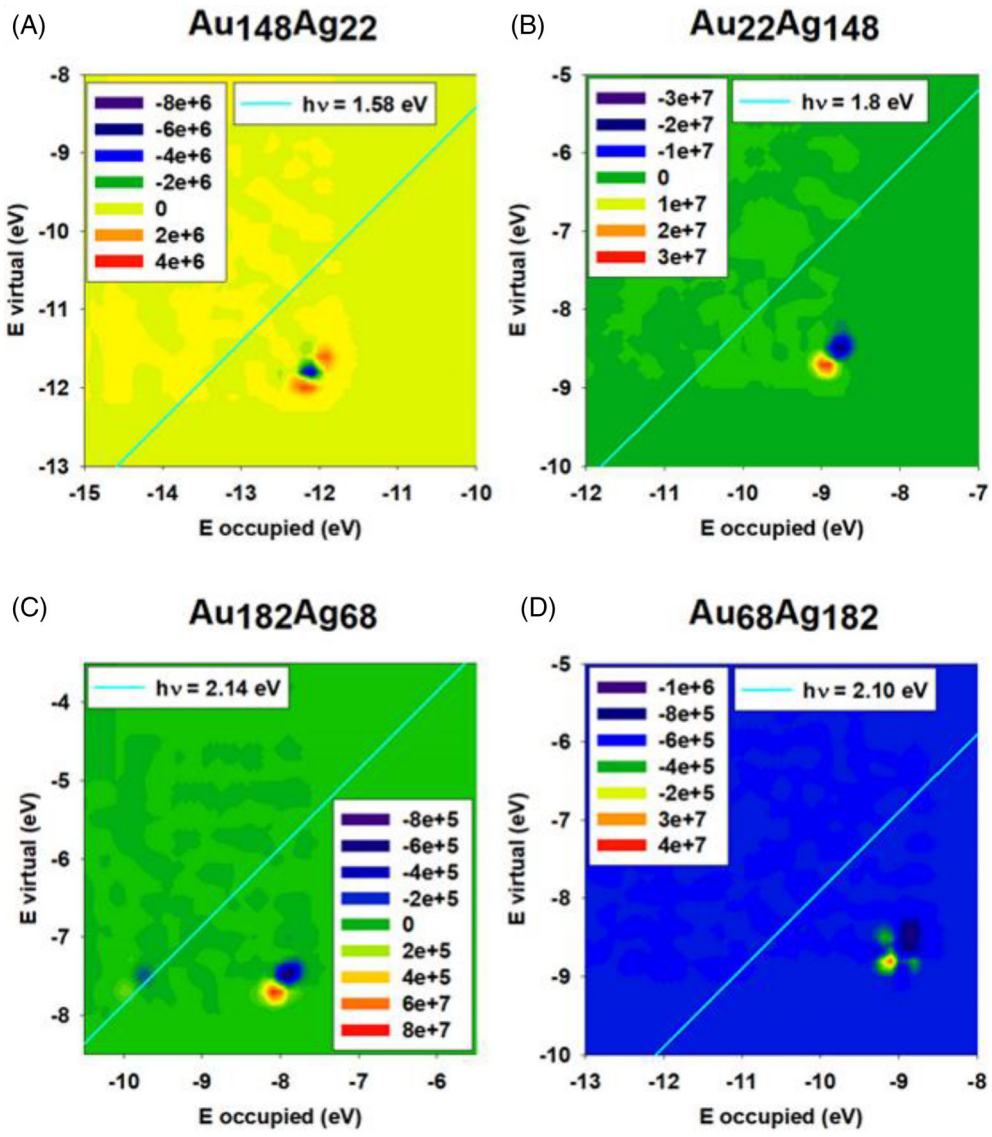

FIGURE 8 ICM-RS analysis of the longitudinal magnetic dipole component at plasmon energies for the 7-1 HMS (A) $Au_{148}Ag_{22}$ and (B) $Au_{22}Ag_{148}$ and the 11-4 HMS (C) $Au_{182}Ag_{68}$ and (D) $Au_{68}Ag_{182}$. The straight line corresponds to virtual-occupied pair energy difference equal to the excitation energy.

sign, so a *partially* destructive interference is taking place. It is interesting to compare this finding to the pure gold (5,3)NT considered previously,[23] also in that case two very strong contributions were present at the plasmon energies, but a *totally* destructive interference was observed, in fact there was basically no appreciable ECD at the plasmon energy. So, we have been able to find out that a proper chemical ordered alloying is effective to "decouple" the *totally* destructive interference by means of alloying the system with silver atoms. It is worth noting, especially in the 3D plots in the right panel of Figure 5, that a large amount of destructive interference is still present, so there is still room to increase the plasmon dichroism, at least in principle. For this reason, it would be important to design or explore additional strategies (besides alloying) to further reduce the amount of destructive interference. Another useful analysis in this context is the inspection of the induced density, as an effect of the external time-dependent perturbation. This analysis is somehow complementary to the ICM-RS, since it is in real-space and therefore more suitable to be visualized and suggest structural changes to improve plasmonic dichroism. In Figure 6, we have considered two different isosurface values, where the larger value of 0.03 electrons/Bohr^3 (Figure 6A,C) shows the localization of the density while the smaller value of 0.00003 electrons/Bohr^3 (Figure 6B,D) is useful to identify a more regular shape. From an inspection of Figure 6, we find the usual dipolar shape, typical of plasmon resonance, but also a curling of the density, especially in the plots with the smaller isosurface value. This finding suggests that, for example, a chiral disposition of protecting ligands around the nanowires should improve the dichroism, favoring a curly induced density. Such a procedure, however, could also quench the plasmon since protective ligands favor the oxidation of the metallic atoms, excluding their active role in the plasmon, so this mechanism might be more promising for larger multiwall nanotubes, which can maintain their plasmonic behavior even in the presence of a ligand shell. It is important to observe that, due to the Cotton profile of the plasmonic dichroism, a fast change in the induced density can be expected for small energy changes near the resonance. We have therefore analyzed the induced density at three very close energy

points: at the maximum positive R, at the plasmon energy, at the maximum negative R. The relative density plots are reported in Figure S1 for $Au_{122}Ag_{30}$ and S2 for $Au_{90}Ag_{62}$ of the Supporting Information. Also in this case two isosurfaces are considered, to facilitate the shape assessment with the small isosurface. The induced density displays actually a phase inversion going through the plasmon, in line with the Cotton profile of the dichroism. Moreover, while the plots with larger isosurface value display a helicity, when the smaller isosurface is considered a very clear-cut helicity is found mainly in the higher energy tail of the plasmon.

A further helpful tool is the fragment analysis, as described in detail in Reference 34. This tool allows one to split the total photoabsorption in partial contributions according to the definition of fragments within the system under study. In practice, for present nanowires it is natural to consider them as built by two fragments: the gold fragment and the silver one. In this case the fragment analysis will assign four partial contributions rising from the four possible transitions: Au → Au, Au → Ag, Ag → Au, and Ag → Ag. Such analysis performed on the two (5,3)NT $Au_{122}Ag_{30}$ and $Au_{90}Ag_{62}$ are reported in Figures S3 and S4 of the Supporting information. Interestingly for $Au_{122}Ag_{30}$ it is evident (Figure S3) that the first plasmonic positive peak of dichoroism can be ascribed to a transition starting and arriving to gold (Au → Au), while the plasmonic negative peak is ascribed to a transition starting from gold and arriving to silver (Au → Ag). Apparently, contributions starting from the silver moiety do not play an important role. For the other nanowire $Au_{90}Ag_{62}$ the analysis (Figure S4) is not helpful since it seems that there is no specific fragment role, it is apparent that the ECD profile is dominated by the Au → Au partial contribution on both side of the plasmonic structure.

We can conclude this subsection saying that, for the first time, we predict theoretically that a dichroic plasmon can be triggered by means of proper alloying.

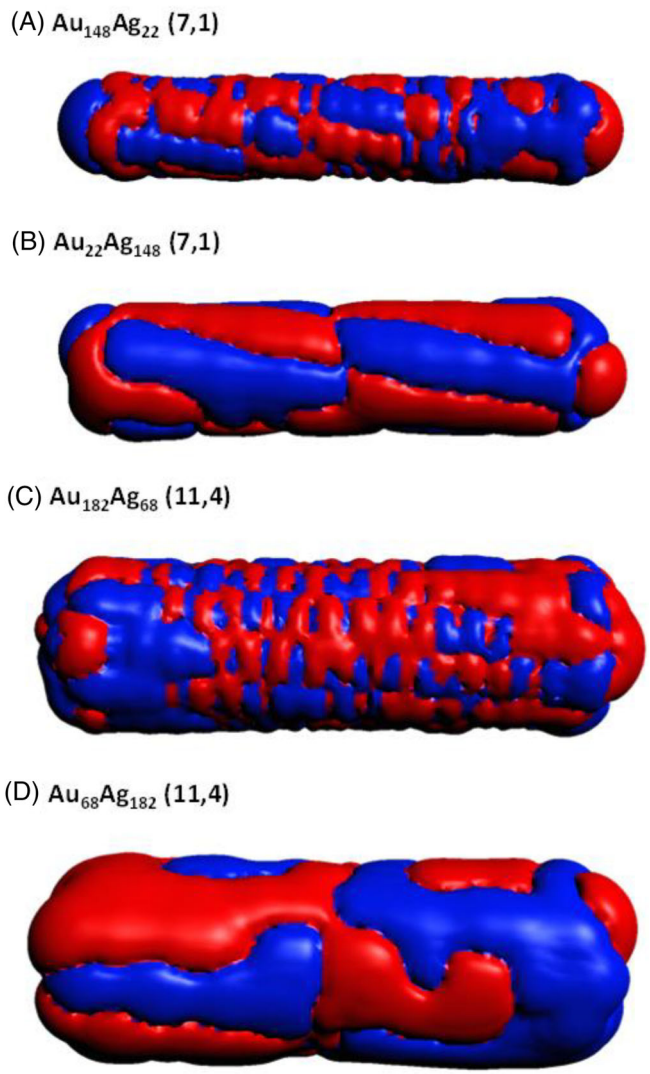

FIGURE 9 The induced density of the longitudinal component at plasmon energies for the 7-1 HMS (A) $Au_{148}Ag_{22}$ and (B) $Au_{22}Ag_{148}$ and the 11-4 HMS (C) $Au_{182}Ag_{68}$ and (D) $Au_{68}Ag_{182}$. The isosurface value is 0.00003 electrons/$Bohr^3$.

3.3 | Nanoalloys plasmonic electronic circular dichroism of 7-1 and 11-4 HMS

In Figure 7, the ECD of the 7-1 and 11-4 HMS nanoalloys are reported. In this case, at variance with the (5,3)NT, we observe a significantly smaller amplification of the ECD at the plasmon energy with respect to the pure nanowire considered in Reference 23. In detail, while the profiles for the 7-1 HMS is rather flat, a small effect can be found for the 11-4 HMS around 2 eV, although in any case it can be observed that the feature around 2.6 eV is larger than the plasmonic one. Moreover the 11-4 HMS response seems to be more sensitive to the chemical ordering than the 7-1 one. To rationalize this somewhat disappointing results, we produced the ICM-RS for the 7-1 HMS $Au_{148}Ag_{22}$, $Au_{22}Ag_{148}$ and 11-4 HMS $Au_{182}Ag_{68}$, $Au_{68}Ag_{182}$ in Figure 8. Once more, we found an almost *total* destructive interference, so in this case the alloying has not been effective in decoupling the contributions and giving rise to a significant plasmonic ECD. If we inspect the induced densities (reported in Figure 9) only for the smaller isosurface value, we find that for the gold exposed systems, Figure 9A,C, the induced density looks rather "granular," while for the silver exposed systems, Figure 9B,D, the density looks much more uniform. This is an effect of the different dynamical behavior of silver with respect to gold: for gold the localized 5d manifolds tends to quench the plasmon, while in silver the behavior is much more typical of a free-electron gas, less sensitive to the fine details of the atomic geometry. In Figures S5 and S6 of the SI we also report the plots obtained with a larger value of the isosurface. An interesting finding is that the curling shape of the induced density, although less evident than in the more active (5,3)NT, shows a kind of "breaking" or "interruption" in the middle of the nanoallys, while when strong plasmonic ECD is calculated (see Figure 6 for comparison) we do not have any "breaking" in the induced density plots. Finally it is important to comment why for (5,3)NT the alloying is efficient in triggering plasmonic dichroism, whereas for 7-1 and 11-4 HMS the alloying strategy fails.

In this respect it is worth noting that in (5,3)NT the alloying consists in doping by Ag one or two strings of atoms which are curling around the longitudinal axis of the system. In contrast, alloying in 7-1 and 11-4 HMS it consists in doping one or four *linear* strings of atoms (not curling) along the longitudinal direction. This suggests that, for doping to be effective in enhancing plasmonic dichroism, it must follow a helical arrangement. This requirement can be rationalized as follows: in pure linear chiral gold nanowires we do not observe plasmonic dichroism because the induced current does not follows the chiral atomic pattern, but rather it moves back and forth following a straight line path. Helical doping forces the induced current to follow a curling path, but this does not happen in 7-1 and 11-4 HMS because in these systems the doping arrangement is linear.

4 | CONCLUSIONS

Here, we have investigated the chiro-optical response of a series of chiral gold/silver alloy nanowires via time-dependent density functional theory (TDDFT) simulations. These systems are promising for chiro-optical sensor applications since they display strong plasmonic optical absorption peaks in a relatively small size. The main conclusion of our study is that by properly alloying silver into chiral gold nanowires, it is possible to trigger a strong plasmonic Electronic Circular Dichroism (ECD) signal, at variance with pure gold nanowire in which a total destructive interference results in a negligible ECD signal at the plasmon energy. A chiro-optically effective alloying is achieved by replacing one or two chains of gold atoms which curl around the axis of the (5,3)NT system. In contrast, alloying an entire single wall (shell) of even larger systems, such as the multiwall 7-1 and 11-4 HMS, is not effective in enhancing the ECD at the plasmon energy, producing less intense ECD peaks. An analysis based on the Individual Component Map of Rotatory Strength (ICM-RS) tool indicates that, whereas in the (5,3)NT system a partial decoupling of destructive contributions from iso-energetic excitations is induced by alloying, in the multiwall case a more significant destructive interference remains. Plots of the induced density further suggest that the plasmon ECD is strong when a curling shape of the density is achieved exhibiting no interruptions along the wire. Further possibilities to remove the phenomenon of destructive interference can then be envisaged from the present analysis, for example by properly adding ligand adsorbates along the helical patterns so as to obtain the desired decoupling of interfering excitations.

ACKNOWLEDGMENTS

Financial support from ICSC—Centro Nazionale di Ricerca in High Performance Computing, Big Data and Quantum Computing, funded by European Union—NextGenerationEU is gratefully acknowledged. This publication is based upon work networked within the COST Action CA21101 "Confined molecular systems: from a new generation of materials to the stars" (COSY) supported by COST (European Cooperation in Science and Technology). Computational support from CINECA supercomputing center within the ISCRA program is gratefully acknowledged. The authors are grateful to the Stiftung Beneficentia for the financial support to set up a computing server. Support from Trieste University within the FRA program is also acknowledged.

DATA AVAILABILITY STATEMENT

The data that support the findings of this study are available from the corresponding author upon reasonable request.

ORCID

Daniele Toffoli https://orcid.org/0000-0002-8225-6119
Mauro Stener https://orcid.org/0000-0003-3700-7903
Luca Sementa https://orcid.org/0000-0002-3951-2842
Alessandro Fortunelli https://orcid.org/0000-0001-5337-4450

REFERENCES

[1] C. Zhang, J. Z. Noguez, *Plasmonics* **2008**, *3*, 127.
[2] M. Rycenga, C. M. Cobley, J. Zeng, W. Li, C. H. Moran, Q. Zhang, D. Qin, Y. Xia, *Chem. Rev.* **2011**, *111*, 3669.
[3] N. Durante, A. Fortunelli, M. Broyer, M. Stener, *J. Phys. Chem. C* **2011**, *115*, 6277.
[4] J. Langer, D. Jimenez de Aberasturi, J. Aizpurua, R. A. Alvarez-Puebla, B. Auguié, J. J. Baumberg, G. C. Bazan, S. E. J. Bell, A. Boisen, A. G. Brolo, J. Choo, D. Cialla-May, V. Deckert, L. Fabris, K. Faulds, F. J. García de Abajo, R. Goodacre, D. Graham, A. J. Haes, C. L. Haynes, C. Huck, T. Itoh, M. Käll, J. Kneipp, N. A. Kotov, H. Kuang, E. C. le Ru, H. K. Lee, J. F. Li, X. Y. Ling, S. A. Maier, T. Mayerhöfer, M. Moskovits, K. Murakoshi, J. M. Nam, S. Nie, Y. Ozaki, I. Pastoriza-Santos, J. Perez-Juste, J. Popp, A. Pucci, S. Reich, B. Ren, G. C. Schatz, T. Shegai, S. Schlücker, L. L. Tay, K. G. Thomas, Z. Q. Tian, R. P. van Duyne, T. Vo-Dinh, Y. Wang, K. A. Willets, C. Xu, H. Xu, Y. Xu, Y. S. Yamamoto, B. Zhao, L. M. Liz-Marzán, *ACS Nano* **2020**, *14*, 28.
[5] M. Barbry, P. Koval, F. Marchesin, R. Esteban, A. G. Borisov, J. Aizpurua, D. Sánchez-Portal, *Nano Lett.* **2015**, *15*, 3410.
[6] L. Sementa, A. Marini, F. R. Negreiros, A. Fortunelli, *ACS Photonics* **2014**, *1*, 315.
[7] S. Bernadotte, F. Evers, C. R. Jacob, *J. Phys. Chem. C* **2013**, *117*, 1863.
[8] R. Zhang, L. Bursi, J. D. Cox, Y. Cui, C. M. Krauter, A. Alabastri, A. Manjavacas, A. Calzolari, S. Corni, E. Molinari, E. A. Carter, F. J. García de Abajo, H. Zhang, P. Nordlander, *ACS Nano* **2017**, *11*, 7321.
[9] R. Sinha-Roy, P. García-González, H. C. Weissker, F. Rabilloud, A. I. Fernández-Domínguez, *ACS Photonics* **2017**, *4*, 1484.
[10] J. H. Mokkath, U. Schwingenschlögl, *J. Chem. Phys.* **2016**, *144*, 134305.
[11] N. J. Halas, S. Lal, W. S. Chang, S. Link, P. Nordlander, *Chem. Rev.* **2011**, *111*, 3913.
[12] N. Kameta, M. Masuda, T. Shimizu, *Chem. Commun.* **2015**, *51*, 11104.
[13] J. J. Pelayo, I. Valencia, A. P. García, L. Chang, M. López, D. Toffoli, M. Stener, A. Fortunelli, I. L. Garzón, *Adv. Phys. X* **2018**, *3*, 1509727. https://doi.org/10.1080/23746149.2018.1509727
[14] N. Karimova, C. M. Aikens, *J. Phys. Chem. A* **2015**, *119*, 8163.
[15] L. Nguyen, M. Dass, M. F. Ober, L. V. Besteiro, Z. M. Wang, B. Nickel, A. O. Govorov, T. Liedl, A. Heuer-Jungemann, *ACS Nano* **2020**, *14*, 7454.
[16] J. M. Slocik, P. B. Dennis, A. O. Govorov, N. M. Bedford, Y. Ren, R. R. Naik, *ACS Biomater. Sci. Eng.* **2020**, *6*, 2612.
[17] Z. Hu, D. Meng, F. Lin, X. Zhu, Z. Fang, X. Wu, *Adv. Opt. Mater.* **2019**, *7*, 1801590.
[18] Z. Fan, A. O. Govorov, *Nanoletters* **2012**, *12*, 3283.
[19] C. Zeng, Y. Chen, C. Liu, K. Nobusada, N. L. Rosi, R. Jin, *Sci. Adv.* **2015**, *1*, e1500425.

[20] S. Lu, L. Xie, K. Lai, R. Chen, L. Cao, K. Hu, X. Wang, J. Han, X. Wan, J. Wan, Q. Dai, F. Song, J. He, J. Dai, J. Chen, Z. Wang, G. Wang, *Natl. Sci. Rev.* **2021**, *8*, nwaa282.
[21] M. E. Casida, in *Recent Advances in Density-Functional Methods* (Ed: D. P. Chong), World Scientific, Singapore **1995**, p. 155.
[22] G. M. Piccini, R. W. A. Havenith, R. Broer, M. Stener, *J. Phys. Chem. C* **2013**, *117*, 17196.
[23] D. Toffoli, A. Russi, G. Fronzoni, E. Coccia, M. Stener, L. Sementa, A. Fortunelli, *J. Phys. Chem. Lett.* **2021**, *12*, 5829.
[24] L. Chang, O. Baseggio, L. Sementa, D. Cheng, G. Fronzoni, D. Toffoli, E. Aprà, M. Stener, A. Fortunelli, *J. Chem. Theory Comput.* **2018**, *14*, 3703.
[25] O. Baseggio, G. Fronzoni, M. Stener, *J. Chem. Phys.* **2015**, *143*, 024106.
[26] O. Baseggio, D. Toffoli, G. Fronzoni, M. Stener, L. Sementa, A. Fortunelli, *J. Phys. Chem. C* **2016**, *120*, 24335.
[27] G. te Velde, F. M. Bickelhaupt, E. J. Baerends, C. F. Guerra, S. J. A. van Gisbergen, J. G. Snijders, T. Ziegler, *J. Comput. Chem.* **2001**, *22*, 931.
[28] R. van Leeuwen, E. J. Baerends, *Phys. Rev. A* **1994**, *49*, 2421.
[29] M. Medves, G. Fronzoni, M. Stener, *J. Comput. Chem.* **2022**, *43*, 1923.
[30] F. Wang, T. Ziegler, E. van Lenthe, S. van Gisbergen, E. J. Baerends, *J. Chem. Phys.* **2005**, *122*, 204103.
[31] O. Baseggio, M. De Vetta, G. Fronzoni, D. Toffoli, M. Stener, L. Sementa, A. Fortunelli, *Int. J. Quantum Chem.* **2018**, *118*, e25769.
[32] S. Theivendran, L. Chang, A. Mukherjee, L. Sementa, M. Stener, A. Fortunelli, A. Dass, *J. Phys. Chem. C* **2018**, *122*, 4524.
[33] Y. Oshima, A. Onga, K. Takayanagi, *Phys. Rev. Lett.* **2003**, *91*, 205503.
[34] L. Sementa, G. Barcaro, O. Baseggio, M. De Vetta, A. Dass, E. Aprà, M. Stener, A. Fortunelli, *J. Phys. Chem. C* **2017**, *121*, 10832.

SUPPORTING INFORMATION

Additional supporting information can be found online in the Supporting Information section at the end of this article.